On the use of laser-induced fluorescence to probe the thermodynamic equilibrium in laser-generated plasmas

Arsène Chemin, Amanda Ross, Sylvain Hermelin, Patrick Crozet, Vincent Motto-Ros, Gilles Ledoux, Christophe Dujardin, David Amans

Graphical Abstract

On the use of Laser-Induced Fluorescence to probe the thermodynamic equilibrium in laser-generated plasmas.

Arsène Chemin, Amanda Ross, Sylvain Hermelin, Patrick Crozet, Vincent Motto-Ros, Gilles Ledoux, Christophe Dujardin, David Amans

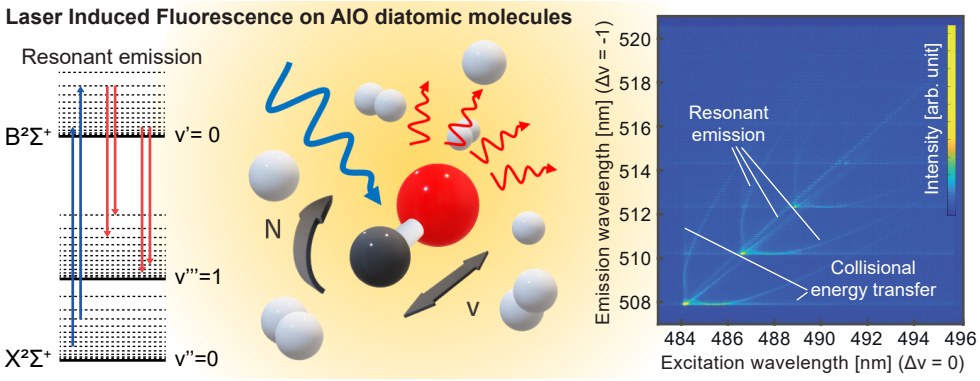

Highlights

On the use of Laser-Induced Fluorescence to probe the thermodynamic equilibrium in laser-generated plasmas.

Arsène Chemin, Amanda Ross, Sylvain Hermelin, Patrick Crozet, Vincent Motto-Ros, Gilles Ledoux, Christophe Dujardin, David Amans

- Determination of ground state rotational temperature from resonant laser-induced fluorescence.
- Rotational temperatures in both ground and excited states are consistent.
- LIF spectra reveal energy redistribution in the excited electronic state with rotational energy transfer up to $\Delta N = -100$.

On the use of Laser-Induced Fluorescence to probe the thermodynamic equilibrium in laser-generated plasmas.

Arsène Chemin[a], Amanda Ross[a], Sylvain Hermelin[a], Patrick Crozet[a], Vincent Motto-Ros[a], Gilles Ledoux[a], Christophe Dujardin[a], David Amans[a,*]

[a] *Univ. Lyon, Université Claude Bernard Lyon 1, CNRS, UMR5306, Institut Lumière Matière, Villeurbanne, F-69100, France*

Abstract

In this work, we investigate thermodynamic equilibria in a laser-generated plasma from ro-vibrational population distributions in the AlO molecule. We address the congruence between the rotational temperatures of diatomic molecules in their excited state and in their ground state, the latter being assumed to correspond to the kinetic temperature of the species in the plasma. The model system consists of AlO molecules produced by ablation of an alumina target in ambient air using a nanosecond laser pulse. Using laser induced fluorescence spectroscopy, we can directly probe the population of the rotational levels in the ground electronic state $X^2\Sigma^+$ of AlO and deduce the corresponding rotational temperature. This temperature is then compared to the population of the rotational levels in the excited state $B^2\Sigma^+$ deduced from the thermal $B - X$ rovibronic emission. In such plasma, AlO molecules in the excited state are believed to be formed by chemical reaction and might be strongly out of equilibrium, but we find that emission from the $B^2\Sigma^+$ excited state provides a useful indication of kinetic temperature of the species in the plasma for delays longer than a few microseconds.

Keywords: Laser-Induced Fluorescence, collisionally induced fluorescence, rovibronic emission, rotation-vibration relaxation, AlO, laser-induced plasma, thermodynamic equilibrium, rotational temperature.

*Corresponding author.
Email address: david.amans@univ-lyon1.fr (David Amans)

1. Introduction

This paper explores just one of the several avenues of study of molecular emission from laser ablation plasmas discussed in the review by Di Giacomo and Hermann [1], exploring non-equilibrium energy distributions in rotational and vibrational degrees of freedom [2]. Measurement of temperatures in laser-generated plasma is a useful diagnostic for the data analysis in laser-induced breakdown spectroscopy (LIBS) [3, 4] and to model nanoparticle growth in the framework of laser-generation of particles such as pulsed laser deposition (PLD) and ablation in air [5], cluster sources [6] and laser ablation in liquids (LAL) [7, 8]. Regarding elemental analysis, diatomic molecules sometimes offer possible advantages in LIBS diagnostics when molecular signatures fall in a more convenient spectral region than the strongest atomic transitions. A particularly striking practical illustration was the diagnostic for fluorine content in minerals via CaF bands, proposed by Alvarez *et al.* [9] in 2014, and successfully applied in the analysis of Martian soil with ChemCam one year later [10].

In this article, we are addressing temperature measurement in AlO molecules, one of the molecular species mentioned in the context of diatomics offering possible advantages in LIBS. We developed a fitting procedure on partially-resolved laser induced fluorescence (LIF) spectra in order to handle separately direct fluorescence (resonant emission, DLIF) and laser-then-collisionally induced fluorescence (LCIF). Using DLIF, we have probed the population of the rotational levels in the ground electronic state $X\Sigma^+$. The rotational temperature of the ground electronic state is then deduced. Using LCIF, We have focused on energy redistribution in the excited $B^2\Sigma^+$ state of AlO.

Regarding the energy redistribution in the excited electronic state, it is well established that there are no selection rules governing collisional energy transfer in a non-symmetric molecule, and a single collision can result in large changes in ΔN and ΔJ, if ΔE commensurate with $k_B T$, even with unreactive collision partners [11, 12]. Changes up to $\Delta J = 70$ have been reported in alkali dimers [13], under controlled conditions of temperature and pressure. Here, more collisional partners are possible, including Al or O atoms, as well as atmospheric oxygen or nitrogen. Spectra reveal extensive rotational energy transfer up to $\Delta J = -100$.

A second issue deals with the measurement of the kinetic temperature of the heavy species in laser generated plasma. An established strategy consists of measuring the rotational temperatures of diatomic molecules from

emission spectroscopy assuming an equilibrium between the internal degrees of freedom of the molecules and the kinetic temperature of the species in the plasma. This is true when molecules are excited by collision with the electrons in the plasma. In that case, the population of the rotational levels in the excited state maps the population of the rotational levels in the ground electronic state, which is supposed to be at equilibrium with the kinetic temperature of the species in the plasma. If molecules are formed in the excited state by chemical reactions, equilibrium may not be achieved if emission lifetimes of the excited state of the molecule are shorter than the characteristic time of collision between the species in the plasma. In such a case, the emission from newly produced diatomic molecules will contribute to the emission spectrum. Hence, the kinetic temperature in transient laser-generated plasma might not match the rotational temperature deduced from the rovibronic emission. Indeed, the imaging of the spatial distribution of AlO emission following the ablation of an Al target or an Al_2O_3 target in air shows a spatial localisation of the emission restricted to the edge of the plasma plume. This observation suggests that the AlO emission comes from the newly-produced molecules at the interface between the plasma plume and the ambient air [14, 15, 16, 17]. To determine if the rovibronic emission from diatomic molecules can be used to assess the kinetic temperature of the species in the plasma, one needs to check the consistency between the temperatures deduced from the rovibronic emission (from plasma emission), characterising the populations in the excited electronic state, and a direct measurement of the rotational temperature (from DLIF) characterising the population of the rotational levels in the ground electronic state.

The synthetic computation of emission spectra for the B-X system of AlO is well described in literature [18, 19] and spectroscopic temperature determination of aluminium monoxide in laser ablation was reported many years ago [20]. Although packages exist to simulate electronic spectra of diatomics, for example PGOPHER [21], ExoMol or programs from Parigger's group [22], we have produced out own routines and developed in house C++ library to compute the spectra (see supplementary materials) and a Matlab program for the fitting procedure.

2. Experimental Set-up

The experimental set-up is described in figure 1. The fourth harmonic of a pulsed Nd:YAG laser (266 nm, 5 ns, 20 Hz, 30 mJ per pulse) is focused

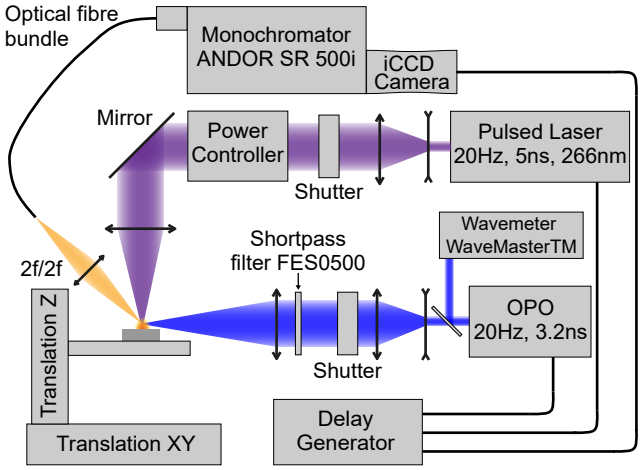

Figure 1: Scheme of the laser induced fluorescence (LIF) experimental set-up.

vertically by a UV lens ($f = 50$ mm) on a mono-crystal of alumina, creating a plasma. The plasma is re-excited by a second laser pulse generated by an NT230-50 Optical Parametric Oscillator (OPO) with SH/SF extension from EKSPLA (NT230 series) using non-linear mixing of an Nd:YAG laser in order to produce broad wavelength coverage (220-1500 nm, 3.2 ns, 20 Hz). A shortpass filter (FES0500, Thorlabs) is introduced on the excitation line to remove any contribution above 500 nm. In the excitation range of the AlO molecules used in this work ($483 - 496$ nm) the laser line-width is 66 pm FWHM (2.6 cm^{-1}). It was measured using a DEMON spectrometer (Lasertechnik Berlin) with a resolution of about 1 pm. The energy per pulse 17 ± 2 mJ was measured with a pyroelectric head on a Nova II energymeter (Ophir). A few percent of the laser beam is sent to a wavemeter WaveMaster^{TM} from Coherent, measuring the excitation wavelength with an accuracy of 5 pm for each LIF spectrum. The beam is focused on the centre of the plasma, about 1 mm above the target surface. Emission from this part of the plasma is collected perpendicularly to the OPO beam path by a 1/2-inch achromatic lens (f=25 mm) imaging about 1 mm of the plasma on a bundle of 19 optical fibres (core diameter of 200 μm) in a $2f/2f$ configuration. Light is diffracted in an Andor Shamrock 500i spectrometer (Czerny-Turner optical design) using a 2400 l/mm (blaze 240 nm) grating and an entrance slit of 10 μm. The spectrometer is equipped with DHT340-25F-03 intensified CCD camera from ANDOR with full vertical binning. The spectrometer is

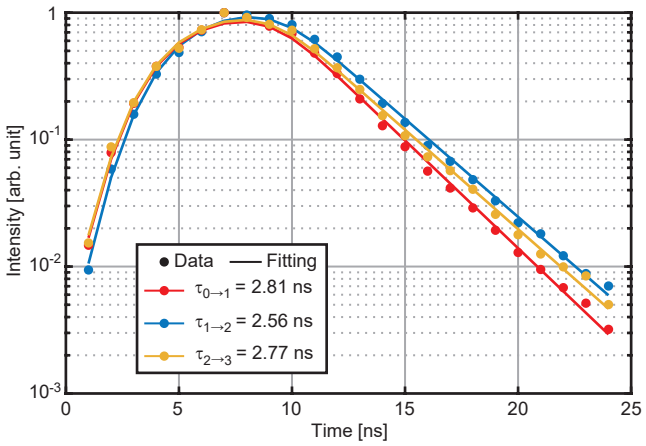

Figure 2: Time dependence of the normalised integrated intensity of the bandheads of three vibronic $B-X$ transitions (v', v'''): red dots correspond to the transition $(0, 1)$, blue dots to $(1, 2)$, and yellow dots to $(2, 3)$. Bandheads are integrated over 0.5 nm. The delay 0 is arbitrary. Solid lines correspond to the fitting procedure described in the text and taking into account the Gaussian excitation pulse, with a pulse width of 3.2 ns FWHM, and a time gate of 5 ns. The deduced emission lifetime for each $v' - v'''$ transition is displayed in the inset.

calibrated before each measurement using scattered light from the OPO at different wavelengths. 22 spectra are recorded by shifting the OPO line by a step of 0.5 nm. For each spectrum, the peak position is fitted by a Lorentzian peak function. The resulting set of measured peak positions is then associated with the set OPO wavelengths and a 3$^{\text{rd}}$ order polynomial fit is used for the calibration. The overall resolution of the acquisition system is 0.05 nm. The gate width is set to 5 ns to reduce the background signal with respect to the LiF signal. The delays between the ablation pulse, the excitation pulse and the measurement are controlled using a digital delay/pulse generator DG645 from Stanford Research Systems. During measurement, the target is moved in the horizontal plane by the translation stage with a precision of about 10 μm and moving at about 1 mm/s. This ensures ablation from a clean surface and provides repeatable ablation conditions and plasma characteristics. The spectral sensitivity response of the system is characterised by measuring a calibrated black body lamp in the exact configuration of the measurement. The measured spectrum is fitted by a 4$^{\text{th}}$ degree polynomial curve and divided by the tabulated spectrum. The resulting correction function is then applied to all the measurements.

3. Quantum numbers and notation

The observed bands belong to the electronic $B^2\Sigma^+ - X^2\Sigma^+$ system of AlO. We use Hund's case b) notation [19], designating the excited state $B^2\Sigma^+$ by a *prime* symbol (n', v', N', J') and the ground state $X^2\Sigma^+$ by a *double prime* symbols (n'', v'', N'', J'') in absorption. *Triple prime* symbols (n''', v''', N''', J''') indicate ground state populations following the $B-X$ rovibronic emission. n stands for the electronic levels. v is the vibrational quantum number and J stands for the quantum number associated with the total angular momentum. $J = N \pm 1/2$ for the $^2\Sigma^+$ electronic states, while N corresponds to the quantum number associated with the rotational angular momentum of the nuclei. The variation of each quantum number A is always given following $\Delta A = A^{upper} - A^{lower}$ (for example, $\Delta J = J' - J''$ or $J' - J'''$), likewise we write (v', v'') for excitation and (v', v''') for emission. Both $X^2\Sigma^+$ and $B^2\Sigma^+$ states have been extensively studied; assignments were straightforward using parameters from Saksena *et al.* [23].

4. Emission lifetime measurements

The lifetime of the $B^2\Sigma^+$ state of AlO molecules is measured 10 μs after the creation of the plasma. This delay was chosen as a good compromise between maximizing the LIF signal and minimizing the plasma emission since the plasma already cooled down significantly. The OPO wavelength is set to 487 nm corresponding to the resonant absorption of the $(1, 1)$ bandhead. The acquisition gating is set to its minimum (5 ns). The delay between the OPO and the acquisition is changed by 1 ns steps and starts about 5 ns before the OPO pulse. Each measurement represents an averaged signal over 100 pulses. Figure 2 displays LIF intensity corresponding to bandheads at 507.9 nm (0,1), 510.2 nm $(1, 2)$, and 512.3 nm $(2, 3)$ integrated over 0.5 nm and normalised with respect to the maximum intensity observed. The excitation pulse and detection gate duration being similar to the deexcitation time of the molecules, their shapes have to be taken into account to fit the emission spectra display in Figure 2. Assuming a non depleted ground state, the excitation rate of the molecules remains proportional to the instantaneous intensity during the whole laser pulse duration. Excitation intensity evolves as a Gaussian function $\mathcal{G}(t)$ with a pulse width of 3.2 ns FWHM. The emission intensity is given by the convolution product of the OPO pulse

intensity and an exponential decay:

$$I(t) = \mathcal{G}(t) \circledast \left[e^{-\frac{t}{\tau}} H(t) \right], \tag{1}$$

with $H(t)$ the Heaviside step function. During the measurement, the emission is integrated over a gate $\Pi(t)$ of 5 ns time duration. The signal recorded $S(t)$ is the convolution product of the Rectangular function $\Pi(t)$ with the emission $I(t)$:

$$S(t) = \Pi(t) \circledast I(t). \tag{2}$$

The solid lines correspond to fits of the data by the function described above. It provides a measurement of the emission lifetime for the three (v', v''') transitions considered: $\tau_{0\to1} = 2.8$ ns, $\tau_{1\to2} = 2.6$ ns, $\tau_{2\to3} = 2.8$ ns. These values are very short compared to the radiative lifetime tabulated by the National Institute of Standards and Technology (NIST), with values from 100 ns [24] to 130 ns [25] for $v' = 0, 1, 2$. Indeed, the typical lifetime from NIST has been measured at low pressure (20 Pa) while our measurements are made at atmospheric pressure. Lifetime of a few nanoseconds has been previously discussed by Nagli et al. [26]. They assume that the shorter lifetime is due to collisional quenchings. Knowing the true effective value is important when using this emission lifetime to determine the ratio of species in the plasma from emission ratios [8, 27], so care is taken to measure the effective emission lifetime in similar conditions.

5. Excitation Emission maps

Emission-excitation maps of atoms and molecules in the laser generated plasma are obtained by changing the excitation wavelength and measuring the emission of the plasma. The delay between the ablation and the OPO pulses is set to 30 μs. The acquisition starts just after the OPO pulse, and the gate width is 5 ns. The wavelength of the OPO is changed from 483 nm to 492 nm in steps of 0.05 nm. This value is similar to the FWHM of the laser. The background spectrum of the plasma emission acquired in the same conditions but without the OPO excitation pulse is subtracted from each spectrum. All the spectra are corrected for the spectral sensitivity of the optical and detection system using the black body calibration. A background contribution determined from the average intensity for $\lambda < 507.5$ nm is also subtracted. The resulting 2D map is presented on figure 3 (c). The largest

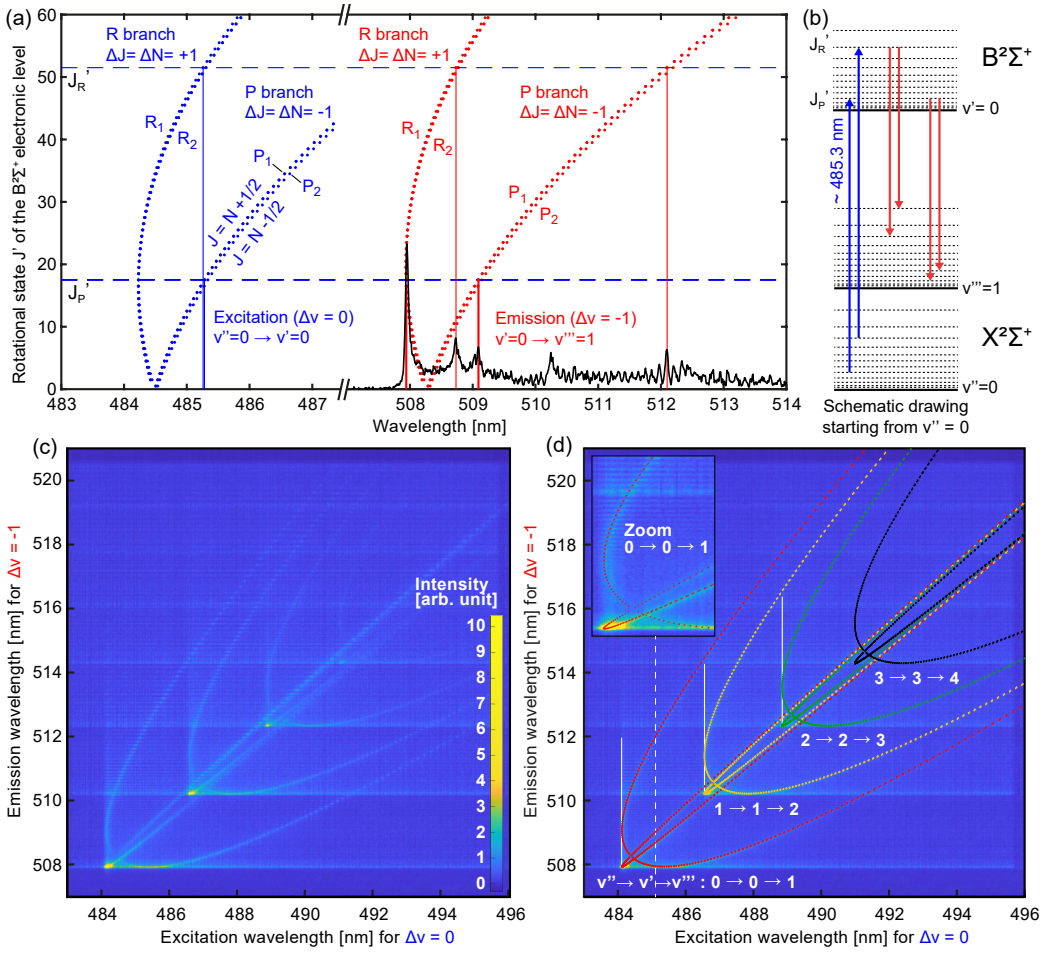

Figure 3: (a) Computed Fortrat diagram for the vibronic $B-X$ transition $(0,0)$ in blue and $(0,1)$ in red. Only the main branches characterised by $\Delta J = \Delta N = \pm 1$ are displayed, i.e. the R_1-branch, R_2-branch, P_1-branch, and P_2-branch. Indexes 1 and 2 correspond to the spin splitting. 1 stands for $J = N + 1/2$ while 2 stands for $J = N - 1/2$. Satellite branches ${}^{P}Q_{12}$ and ${}^{R}Q_{21}$ are not displayed because their intensity is weak for large J' values with respect to the intensity of the R-branch and P-branch. A given excitation wavelength can excite a few states (v', N', J') in the R-branches and P-branches. As an illustration, for an absorption around 485.3 nm (vertical blue line), we highlight two excited states $(0, N'_R, J'_R = N'_R + 1/2)$ and $(0, N'_P, J'_P = N'_P + 1/2)$. Each excited state leads to two emission lines (red vertical lines), one corresponding to a the R-branch and one corresponding to a P-branch. The highlight emission lines appear in the LIF spectrum (black). (b) Same example represented on an energy level scheme with arrows displayed for the resonant emission (DLIF). (c) 2D excitation/emission of an AlO molecule for a delay of 30 μs. (d) Superposition of the 2D excitation/emission spectrum with theoretical transitions assuming resonant excitation and emission from the (v', N', J') state. Satellite branches ${}^{P}Q_{12}$ and ${}^{R}Q_{21}$ are not displayed. The spectrum displayed in (a) corresponds to the white dashed line. Intersection with the four red branches correspond to the four emission peaks highlighted in (a) and (b). Vertical white lines show collisionally induced fluorescence following absorption in the bandheads $\Delta v = 0$.

intensities correspond to the the R-branch heads in absorption and emission. A bandhead is characterised by a large density of nearly-overlapping rovibronic transitions (See Fortrat diagram 3 (a)). In the excitation-emission map, a large density of transitions leads to intense emissions at 507.9 nm, corresponding to the bandhead of the (0,1) R-branch, following an excitation at 484.2 nm, corresponding to the bandhead of the (0,0) R-branch. In the same way, an intense emission is observed at 510.2 nm following an excitation at 486.7 nm (bandhead of (1,2) and (1,1) transitions), as well as at 512.3 nm following an excitation at 488.9 nm (bandhead of (2,3) and (2,2) transitions). Furthermore, the transitions involving low vibrational levels, namely (0,0) excitation and (0,1) de-excitation, have a larger intensity, reflecting enhanced populations, and large Franck-Condon factors (for (0,0) at least).

The curved branches on figures 3 (c) and (d) correspond to direct fluorescence from the rotational states J' populated by the resonant OPO pulse excitation according to transition enabled by selection rules. For AlO $B^2\Sigma^+ - X^2\Sigma^+$ system, these include $\Delta N = \Delta J = \pm 1$ corresponding to the four branches R_1, R_2 and P_1, P_2 represented in blue on figure 3 (a). The spin component F_1 indicates levels $J = N + 1/2$, and F_2 $J = N - 1/2$. R-branches correspond to $\Delta J = +1$. P-branches correspond to $\Delta J = -1$. In the case of AlO, the satellite branches ${}^PQ_{12}$ and ${}^RQ_{21}$ corresponding to $\Delta N = \pm 1$ and $\Delta J = 0$ are almost lost beneath the $\Delta N = \Delta J$ R and P branches. For $J > 5$, their intensities are at least 100 times lower than those of the main branches R and P. For simplicity, they are not plotted on the figures, but are taken into account when fitting the spectra.

In figure 3, excitation is performed in the $\Delta v = 0$ sequence while emission is observed in the spectral range $\Delta v = -1$. A given excitation wavelength can excite a few states (v', N', J') in the R-branches and P-branches according to the laser line-width. As an illustration, two states excited by 485.3 nm photons are highlighted in figure 3 (a) by the vertical blue lines, one in the R_1 branch and one in the P_1 branch for $(v', v'') = (0, 0)$. Assuming spin conservation, and looking at the transitions $\Delta v = -1$, each of these two excited states can decay by spontaneous emission through 2 channels following the selection rules $\Delta N = \Delta J = \pm 1$, *i.e.* one in the R-branch and one in the P-branch. In this example, it leads to 4 transitions indicated by the red vertical lines on figure 3 (a). The black spectrum in figure 3 (a) corresponds to a measured spectrum for an excitation at 485.3 nm. One can observe 4 groups of transitions centred around 507.95, 508.7, 509.1 and

512.1 nm. This relaxation scheme applied on all excitation wavelengths leads to the 4 red branches for $v' = 0$ in the excitation/emission map on figure 3 (d). The example given in figure 3 (a) corresponds to the white dashed line of figure 3 (d). This reasoning also stands for the other vibrational levels and the branches are represented in yellow for $v' = 1$, green for $v' = 2$ and black for $v' = 3$. The inset in figure 3 (d) corresponds to a zoom on the wavelength ranges corresponding to the bandhead transitions for (0,0) excitation and (0,1) emission. It shows the good agreement between the measured spectrum and the transition conserving J'.

The branches highlighted on figure 3 (d) correspond to direct fluorescence, but no matter the excitation wavelength, some excited molecules undergo inelastic energy transfer, spreading the population in the rotation and vibration quantum numbers. The black spectrum on figure 3 (a) clearly exhibits collisionally induced fluorescence in addition to direct fluorescence. Collisionally induced fluorescence especially leads to bright horizontal lines and vertical lines on figure 3 (c). Vertical lines correspond to bandheads $\Delta v = 0$ in absorption. They are shown with vertical white line in figure 3 (d). For instance 484.2 nm corresponds to the (0,0) bandhead, 486.7 nm to the (1,1) band-head and so on. For an excitation wavelength at a bandhead, the light absorption is drastically increased because many transitions are excited simultaneously, populating multiple (v', N', J') levels, and then the collisionally induced fluorescence signal increases accordingly. Horizontal lines correspond to bandhead exaltation with $\Delta v = -1$. We observe that regardless of the excitation wavelength, the collisionally induced fluorescence is concentrated around bandhead wavelengths simply because of a larger density of lines. In particular, one can notice horizontal lines corresponding to emission bandheads at 507.9nm for the (0,1) transitions, 510.2 nm for the (1,2) transitions, 512.3 nm for the (2,3) transitions and so on.

Such Excitation/Emission maps show that, despite dense plasmas and large collision rates, one can observe emission from partially thermalised molecules exhibiting clear patterns according to selection rules of transitions. These 2-D patterns resemble Fortrat diagrams and could be used to determine the validity of molecular constants in hot states (above 3000 K). Our measurements match well the tabulated values for AlO within the precision of the presented measurements.

The lowest horizontal line corresponding to (0,1) bandhead emission at 507.8 nm appears following excitation anywhere out to 496 nm, where the laser is resonant with $J'' > 120$ transitions in the (0,0) band, and lower J''

transitions in (1,1), (2,2) or (3,3) hot bands. Collisional energy transfer is responsible for transferring these excited state populations down to $v' = 0$, $J' \approx 20$, with $\Delta J'$ as much as -100, and $\Delta v'$ = -1, -2, -3. Gain in energy is evident, too, as illustrated by the vertical line formed following (0,0) laser excitation at 484.2 nm, extending to 512.3 nm. In this case, the emission signal comes from molecules in $v' = 0$ vibrational state with J values larger than 60, implying rotational energy transfer up to $\Delta J = +40$, or from molecules with v up to 2, corresponding to vibrational energy transfer up to $\Delta v = +2$. Horizontal lines for excitation wavelengths shorter than an excitation bandhead $\Delta v = 0$ reveal vibrational energy transfer. As an example, emission at 514.3 nm in the bandhead for the (3,4) transitions after excitation at 485 nm is only possible if there is a collisional energy transfer from $v' = 0$ to $v' = 3$. There are no selection rules governing collisional energy transfer in a non-symmetric molecules. These experiments with selective excitation and detection give direct evidence for collisional energy transfer propensities in AlO.

6. LIF spectrum simulation

In order to calculate the LIF spectrum, one has to consider both the excitation and de-excitation processes between the $X^2\Sigma^+$ (n'', n''') and $B^2\Sigma^+$ (n') electronic states. The LIF spectrum can be described as the superposition of direct fluorescence (DLIF), where the excited state (n', v', J', N') involved in the absorption and the emission is the same (resonant fluorescence), and laser-then-collisionally induced fluorescence (LCIF) after collisional population transfer in the excited state (ro-vibrationally relaxed fluorescence). The population redistribution can be approximated by independant vibrational and rotational Boltzmann distributions. By fitting spectral profiles to a linear combination of both combributions to LIF spectra, direct fluorescence and collisionally induced fluorescence, we are able to determine effective temperatures describing the populations in the rotational and vibrational manifolds of X and B states independently. We are following formalisms available in standard textbooks [19, 28, 29].

To calculate the direct fluorescence spectrum, we consider the following excitation/de-excitation channel:

$$(n'', v'', N'', J'') \rightarrow (n', v', N', J') \rightarrow (n''', v''', N''', J''') \tag{3}$$

In the following, the set of quantum numbers (n, v, N, J) is noted l in the equations. The population of the ground state n'' ($X^2\Sigma^+$) is described by a rotational and vibrational temperatures T''_{rot} and T''_{vib} such that the density of molecules in the state (n'', v'', N'', J'') is:

$$N_{l''} = \frac{N_{n''}}{2} \cdot (2J''+1) \cdot \frac{exp\left(-\frac{hc \cdot G_{n''}(v'')}{k_B \cdot T''_{vib}}\right)}{Qvib_{n''}(T''_{vib})} \cdot \frac{exp\left(-\frac{hc \cdot F_{n'',v'',i}(J'')}{k_B \cdot T''_{rot}}\right)}{Qrot_{n'',v''}(T''_{rot})} \tag{4}$$

with $N_{n''}$ the total population of the electronic state, Q the partition functions, G the vibrational energy, and F the rotational energy. i corresponds to the spin splitting. $i = 1$ stands for $J = N + 1/2$ and $i = 2$ stands for $J = N - 1/2$. Considering only transitions from the $X^2\Sigma^+$ electronic state, $N_{n''}$ and $Qvib$ are assumed constant. Since we have $kT_{rot} \gg B_{n'',v''}$ (with $B_{n'',v''}$ the rotational constant for the state (n'', v'')), $Qrot$ is approximated using the rigid rotator model [27]:

$$Qrot_{n'',v''} \simeq \frac{k_B T_{rot}}{B_{n'',v''}}, \tag{5}$$

and from equation 4,

$$N_{l''} \propto (2J''+1) \cdot \frac{B_{n'',v''}}{k_B T''_{rot}} \cdot exp\left(-\frac{hc \cdot G_{n''}(v'')}{k_B \cdot T''_{vib}}\right) \cdot exp\left(-\frac{hc \cdot F_{n'',v'',i}(J'')}{k_B \cdot T''_{rot}}\right) \tag{6}$$

The population of the upper state (n', v', N', J') is considered to be zero prior to excitation. This is not strictly true, but remaining plasma emission is very much weaker than LIF signal at the delay considered, and in any case the plasma emission contribution is subtracted from LIF spectra in our data processing. Considering only the absorption of the excitation pulse, the population variation of the upper state $N_{n',v',J'}$ is:

$$\frac{dN_{l'}}{dt} = \rho(\nu) \cdot B^{l'}_{l''} \cdot N_{l''} \tag{7}$$

with $B_{l''}^{l'}$ the Einstein coefficient for absorption and $\rho(\nu)$ [J.s.m^{-3}] the radiance of the OPO pulse at the resonant wavelength. ν stands for the wavenumber of the transition. The population of the upper state is given by the integration of this transition rate over the duration of the OPO pulse. The radiance $\rho(\nu)$ is assumed undepleted on the whole plasma plume. The number of molecules in the ground state being large compared to the number of molecules excited by the pulse, one can consider that $N_{l''}$ remains constant. The Einstein coefficient for absorption can be related to the Einstein coefficient for spontaneous emission $A_{n'',v''}^{n',v'}$ through the following relation:

$$B_{l''}^{l'} = \frac{(2J'+1)}{(2J''+1)} \frac{c^3}{8\pi h\nu^3} A_{n'',v''}^{n',v'} \frac{S_{J''}^{J'}}{2J'+1} \tag{8}$$

$S_{J''}^{J'}$ denotes the Hönl-London coefficient [19]. Combining equation 6, 7 and 8 we obtain the number of molecules in the excited state after the pulse absorption:

$$\begin{aligned} N_{l'} \propto & \frac{\rho(\nu)}{\nu^3} \cdot A_{n'',v''}^{n',v'} \cdot S_{J''}^{J'} \cdot \frac{B_{n'',v''}}{k_B T''_{rot}} \\ & \cdot exp\left(- \frac{hc \cdot F_{n'',v'',i}(J'')}{k_B \cdot T''_{rot}} \right) \cdot exp\left(- \frac{hc \cdot G_{n''}(v'')}{k_B \cdot T''_{vib}} \right) \end{aligned} \tag{9}$$

The emission intensity from the state (n', v', N', J') to (n''', v''', N''', J''') is thus proportional to the population of the excited state multiplied by the Einstein coefficient for spontaneous emission $A_{n''',v'''}^{n',v'}$:

$$\begin{aligned} I_{l'''}^{l'} & \propto A_{n''',v'''}^{n',v'} \cdot \frac{S_{J'''}^{J'}}{(2J'+1)} \cdot N_{n',v',J'} \\ I_{l'''}^{l'} & \propto \frac{\rho(\nu)}{\nu^3} \cdot A_{n''',v'''}^{n',v'} \cdot A_{n'',v''}^{n',v'} \cdot \frac{S_{J'''}^{J'} \cdot S_{J''}^{J'}}{(2J'+1)} \frac{B_{n'',v''}}{k_B T''_{rot}} \\ & \times exp\left(- \frac{hc \cdot F_{n'',v'',i}(J'')}{k_B \cdot T''_{rot}} \right) \cdot exp\left(- \frac{hc \cdot G_{n''}(v'')}{k_B \cdot T''_{vib}} \right) \end{aligned} \tag{10}$$

Within the effective excited state life-time, the excited state (n', v', N', J') population is partially redistributed over other quantum levels. Because of the limited experimental resolution, the population redistribution of excited states cannot be determined directly from spectral analysis. Here we chose

to model the population after relaxation using two Boltzmann distributions with effective temperatures T'_{vib} and T'_{rot} for vibration and rotation. One should consider these temperatures as fitting parameters. The higher these parameters, the larger the population in states with high quantum levels. The intensity of each transition is proportional to:

$$I^{l'}_{l'''} \propto A^{n',v'}_{n''',v'''} \cdot S^{J'}_{J'''} \cdot \frac{B_{n',v'}}{k_B T'_{rot}} \cdot exp\left(- \frac{hc \cdot F_{n',v',i}(J')}{k_B \cdot T'_{rot}} \right) \cdot exp\left(- \frac{hc \cdot G_{n'}(v')}{k_B \cdot T'_{vib}} \right) \tag{11}$$

The energy of each state, including the electronic energy, the vibrational energy $G_n(v)$ and the rotational energy $F_{n',v',i}(J')$, is computed using the data from Saksena *et al.* [23] (See supplementary materials). The rotational constant $B_{n,v}$ are also taken from Saksena *et al.* [23]. Figures 3 (a) and 5 (a) show Fortrat diagrams calculated for electric-dipole allowed transitions between these states, verifying predicted wavenumbers with the lines lists given by Launila and Berg [30]. Each spectrum is calculated by summing the contribution of all allowed transition convoluted by a Gaussian function of width σ, and using the Einstein coefficient $A^{n',v'}_{n'',v''}$ (and $A^{n',v'}_{n''',v'''}$) from Hebert and Nicholls [31]. Both direct fluorescence (DLIF) spectrum and laser-then-collisionally induced fluorescence (LCIF) spectrum are normalised by their integral over the wavelength range. The final spectrum is the sum of both contributions, weighted by coefficient x:

$$I = x \times \frac{I_{LCIF}}{\int I_{LCIF}} + (1 - x) \frac{I_{DLIF}}{\int I_{DLIF}} \tag{12}$$

x is the fraction of the collisionally induced fluorescence with respect to the total emission. The closer the value of x to one, the more important is relaxation in the excited electronic state.

7. LIF spectrum fit and results

Band contour fits have been performed for each excitation wavelength λ_e corresponding to the measured wavelength of the OPO pulse. The curve-fitting is performed using functions available in Matlab to solve nonlinear

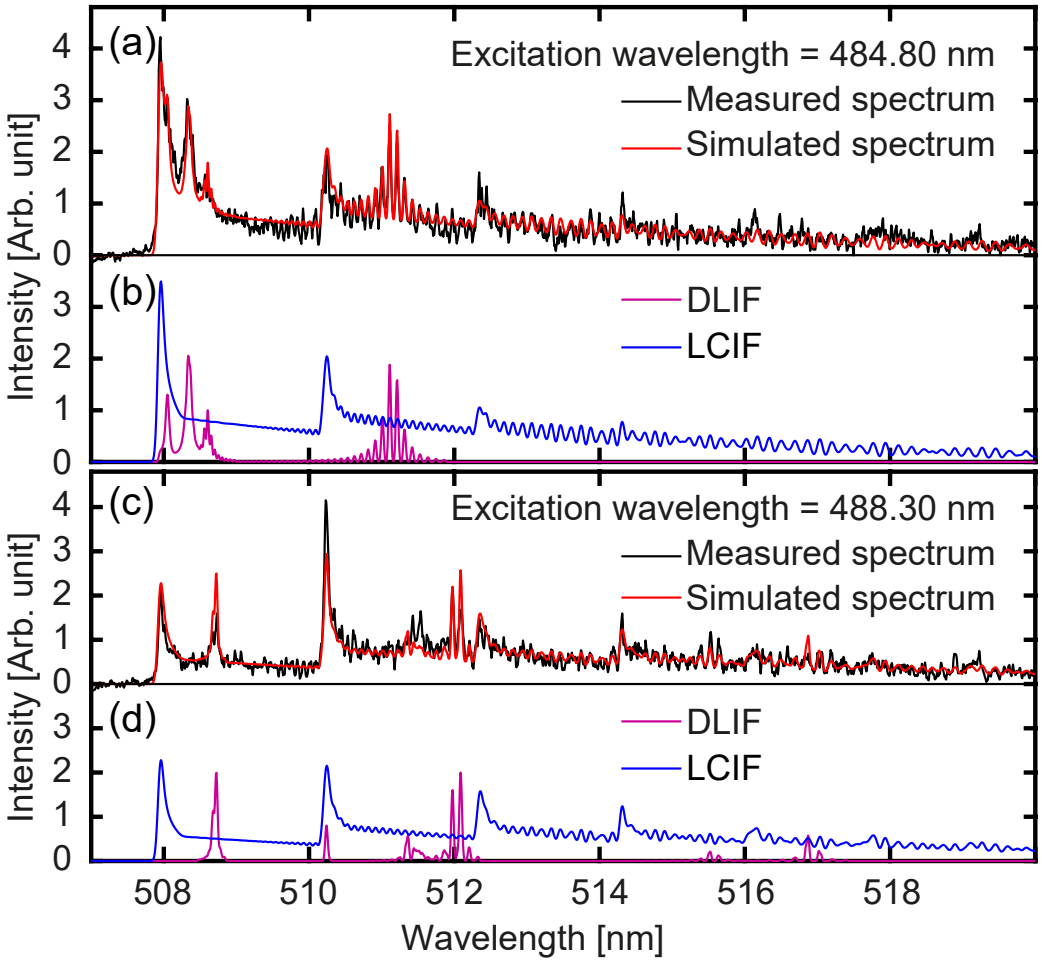

Figure 4: Example of fitted LIF spectrum (red) on measured spectrum for a delay of 30 μs (black) for the excitation wavelength 484.80 nm (a) and 488.30 nm (c) considering a single temperature $T_{X^2\Sigma^+}$ for the electronic ground state $X^2\Sigma^+$, and two temperatures, T'_{rot} and T'_{vib}, for the electronic excited state $B^2\Sigma^+$. Fitted values at 484.80 nm are T'_{rot} = 4520 K, T'_{vib} = 1330 K, and $T_{X^2\Sigma^+}$ = 2380 K. Fitted values at 488.30 nm are T'_{rot} = 4450 K, T'_{vib} = 2970 K, and $T_{X^2\Sigma^+}$ = 2720 K. Panels (b) and (d) show the collisionally induced fluorescence contribution in blue (LCIF) and the direct fluorescence contribution in magenta (DLIF) for each excitation wavelength.

least-squares regression. The radiance of the OPO pulse $\rho(\nu)$ is taken proportional to a Lorentz function centered on λ_e with a line-width of 66 pm FWHM. The fitting parameters are $T_{X^2\Sigma^+}$ describing the population in the $X^2\Sigma^+$ state, T'_{rot} and T'_{vib} describing the population in the $B^2\Sigma^+$ relaxed state, the width σ of the Gaussian function used to compute the synthetic spectra and the ratio x defined in equation 12. The average value of the fitted σ is 0.084 nm (FWHM) with a standard deviation of 0.006 nm. $T''_{rot} = T''_{vib} = T_{X^2\Sigma^+}$ is assumed in the fitting process as we consider the equilibrium for the molecules in the ground state to be reached. Leaving both parameters free in the optimisation process is not relevant as T''_{vib} has little effect on the shape of the emission for the $\Delta v = 0$ transitions we measured here. In order to fit both temperatures of the ground state, one should consider exciting other transitions such as $\Delta v = \pm 1$. Furthermore, for excitation wavelengths lower than 486.5 nm, v" $= 0$ is the only excited state and the fit does not depend on T''_{vib}.

Figures 4 (a) and (c) represent the calculated LIF spectrum (in red) fitted on the LIF spectrum measured (in black) for an excitation of 484.80 nm and 488.30 nm respectively. Figure 4 (b) and (d) represent the direct fluorescence contribution in magenta and the collisionally induced fluorescence contribution in blue in the calculated spectrum. The calculated LIF spectrum accurately reproduces the shape and intensities of the measured LIF spectrum. On this spectral range, direct fluorescence represents only 6 to 16% of the integrated intensity signal. However, direct fluorescence remains easy to identify in tight spectral windows. Most of the intensity, about 90%, corresponds to collisionally induced fluorescence. Despite the short lifetime of the excited state (2.7 ns), collisions efficiently redistribute population amongst excited states v' and J'.

Results of the fitted temperatures for each excitation wavelength are displayed on figure 5. Figure 5 (a) shows the Fortrat diagram of AlO molecules in the excitation range $\Delta v = 0$, from $v' = v'' = 0$ to $v' = v'' = 4$. Vertical dashed lines in figures 5 (a) and (b) indicate bandheads. Figure 5 (b) shows plots of fitted T'_{rot} and T'_{vib} describing the relaxed excited state.

Wavelengths below 484.2 nm cannot excite any bands in the $\Delta v = 0$ sequence, but may be resonant with $\Delta v = +1$ transitions with large values of J''. We find $T'_{rot} \simeq 6000\ K$ and $T'_{vib} \simeq 4500\ K$. Collisionally-induced fluorescence retains some memory of the excitation channel. Initial excitation of high values of J' and v' always results in high T'_{rot} and T'_{vib} temperatures

(obvious in the right hand side of figure 5 (b)).

Between 484.2 nm and 486.5 nm, the $(0,0)$ transitions are excited, leading to a strong LIF signal. $T'_{vib} \simeq 1000\ K$ is much lower here because only the lower vibrational level $v' = 0$ is excited. After mixing, most of the molecules remain in a low vibrational state, leading to a low effective vibrational temperature. Around 484.2 nm, the rotational temperature T'_{rot} drops to $\simeq 4000\ K$ because the excitation corresponds to the $(0,0)$ bandhead with a large density of rovibronic transition with low values of J. Then, T'_{rot} increases between 484.2 nm and 486.5 nm as the excited transitions have larger and larger values of J.

Between 486.7 nm and 488.8 nm, both $(0,0)$ and $(1,1)$ transitions are excited, leading to a higher T'_{vib}. At 486.7 nm, the density of $(1,1)$ transition is large (bandhead) and most of the excited molecules end in this vibrational state explaining the peak in the vibrational temperature. On the contrary, the rotational temperature first drops before increasing for the same reason as presented for pure $(0,0)$ transitions. The amplitude of the variation is weaker as there are also contibutions from the high-J resonances in the $(0,0)$ band, giving more "strating point" for collisional energy transfers. This pattern for T'_{rot} and T'_{vib} repeats for each of the excited (v', v'') bands.

Figure 5 (c) shows the fitted temperatures $T_{X^2\Sigma^+}$ for the ground state. For each OPO pulse centred on an excitation wavelength away from the bandhead, at least two sets of J" values are excited, one belonging to R-branch and the other to the P-branch. The large difference between these two sets of J" numbers allows obtaining a value of $T_{X^2\Sigma^+}$ for each excitation wavelength longer than 485 nm. For wavelengths longer than 490 nm, the direct fluorescence signal is too weak to achieve convergence and deduce $T_{X^2\Sigma^+}$. Figure 5 (c) shows that $T_{X^2\Sigma^+}$ remains stable as it depends on the plasma thermodynamic state only, and not on the excitation process. One can notice a slight peak for the $(1,1)$ bandhead, but also for the $(2,2)$ bandhead. In this region, large resonant intensity and self-absorption might impact the fitting procedure, but the possible consequences of an optically thick sample are not considered here. To determine the temperature of the ground state, we average $T_{X^2\Sigma^+}$ values from excitation wavelength between 485 and 486.5 nm (shaded area in figure 5 (c)). In that range, the emission shape does not depend on T''_{vib} since only one vibrational state is involved, and we then assume $T_{X^2\Sigma^+} = T''_{rot}$. The histogram for the $T_{X^2\Sigma^+}$ distribution from the shaded area is plotted in figure 5 (d). The average value is 3150 K, the

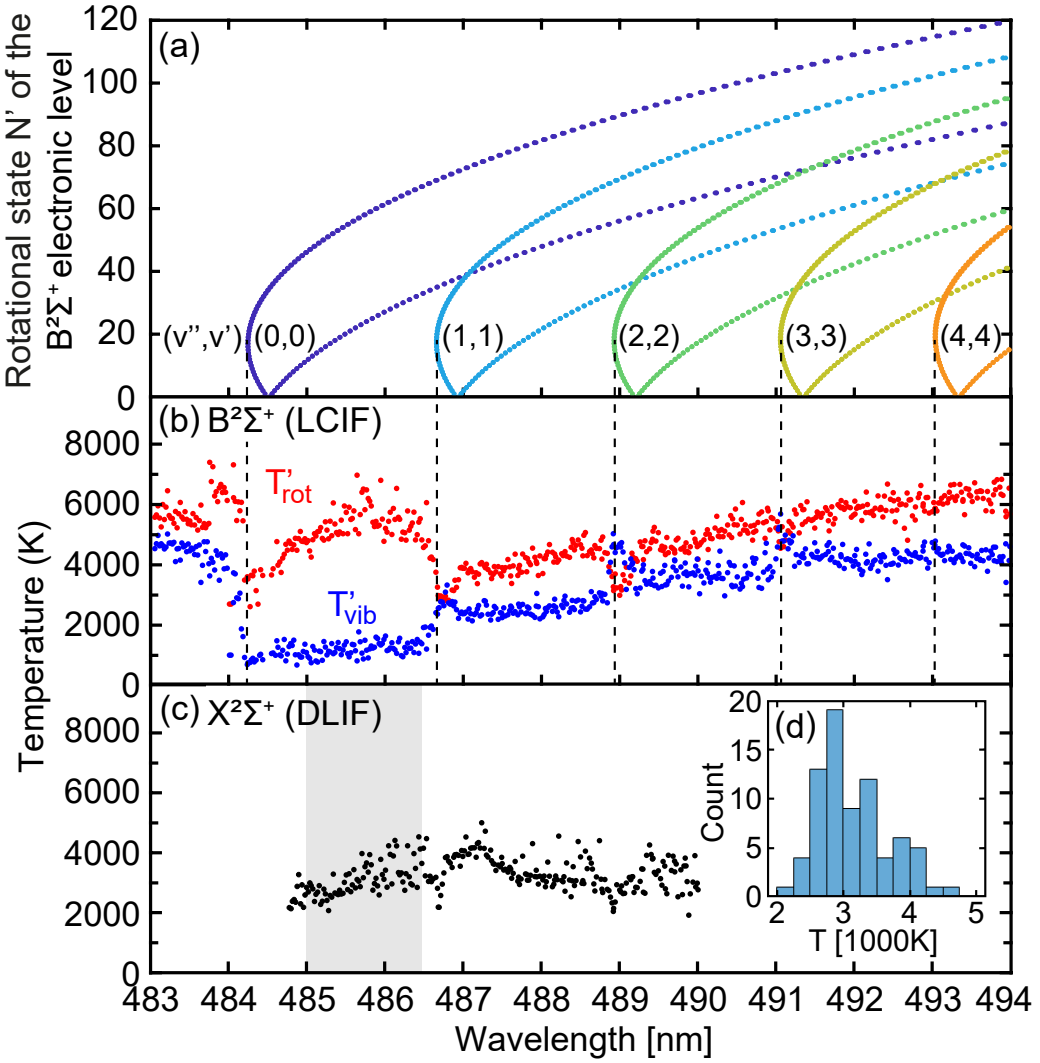

Figure 5: (a) Fortrat diagram for the $\Delta v = 0$ excited transitions. (b) Rotational (red) and vibrational (blue) temperatures describing the collisionally induced fluorescence (LCIF) depending on the excitation wavelength. (c) Temperature of the ground state ($X^2\Sigma^+$) depending on the excitation wavelength measured from the direct fluorescence (DLIF). (d) Histogram of the ground state ($X^2\Sigma^+$) temperatures corresponding to the selected excitation range shaded area. The average value is 3150 K, the standard deviation is 552 K and the temperature interval for a confidence level of 70% (two-sided) is ±67 K.

standard deviation is 552 K and the temperature interval for a confidence level of 70% (two-sided) is ±67 K.

This temperature can be compared to the vibrational and rotational temperatures of the $B^2\Sigma^+$ excited state measured from emission spectroscopy. Emission of AlO molecules has been measured before and after the 2D scanning without OPO excitation and fitted as presented in the supplementary materials following the method presented in Lam *et al.* [27]. The value obtained for the vibrational temperature is 5620 ± 330 K (confidence level of 70%) at a delay of 30 μs. The value obtained for the rotational temperature is 3130 ± 100 K. The rotational temperature of the excited state $T_{rot}^{B^2\Sigma^+}$ is in good agreement with the rotational temperature of the ground state $T_{X^2\Sigma^+}$ measured by LIF. These measurements confirm that after 30 μs, the measurement of the rotational temperature of the excited state from the emission of the plasma is a good probe of the rotational temperature of the ground state.

In order to test it for shorter delay time in the plasma, the same experiment was run with a delay of 5 μs. The average value of $T_{X^2\Sigma^+}$ is 3700 K, the standard deviation is 530 K and the temperature interval for a confidence level of 70% (two-sided) is ±64 K. $T_{X^2\Sigma^+}$ at 5 μs is larger than after 30 μs as the plasma cools down. In comparison, the direct fluorescence provides a vibrational temperature of the excited state $T_{vib}^{B^2\Sigma^+} = 6860 \pm 350$ K (confidence level of 70%) and a rotational temperature of $T_{rot}^{B^2\Sigma^+} = 3850 \pm 100$ K. Here again, the values are in agreement considering the error of the measurement. These temperatures are consistent with the ones reported for AlO molecular temperatures for the same delay in laser-generated plumes from metals [32].

8. Conclusion

We used time resolved 2D LIF to study the out-of-equilibrium properties of excited AlO molecules formed in a laser-generated plasma. Laser induced plasmas are usually characterised using emission spectroscopy to determine temperature and composition. This approach probes only the excited state of the molecules that are likely to be directly formed in the plasma. Ground-state distributions are likely to be different. By tuning a laser to chosen molecular transitions, we can probe rovibrational distribution in the ground state as well.

LIF was used to measure the effective lifetime $\tau = 2.7 \pm 0.2$ ns of the $B^2\Sigma^+$ state of AlO molecules at atmospheric pressure. This lifetime is much

shorter than tabulated values in vacuum because of collisional quenching in the plasma. Effective lifetimes are key parameters for the calculation of molecular concentrations in LIBS.

By fitting both direct and collisionally induced fluorescence contributions to spectra of AlO molecules 5 μs and 30 μs after ablation, we were able to determine the temperature of the ground electronic state of AlO($X^2\Sigma^+$) and the effective temperatures describing the relaxed state of the molecules partially thermalised. Their population appears to be well described by Boltzmann populations using effective rotational and vibrational temperatures. These temperatures are different, and depend on excitation channel. Clearly molecules do not reach full internal equilibrium, or equilibrium with the plasma kinetic temperature. In such a plasma, collisions are not sufficient to ensure equilibrium of the excited molecule population from an initial state strongly out of equilibrium.

On the contrary, the rotational temperature deduced from standard plasma emission, without re-excitation of the plasma, is consistent with the rotational temperature of the ground state deduced from LIF, both after 5 μs and 30 μs. The AlO molecules formed in the excited state $B^2\Sigma^+$ in the plasma reach the equilibrium before emission. This might be because they are not formed far from equilibrium, unlike the molecules excited by LIF. The measurement of the temperature in the plasma considering the rotational temperature of the excited state of the diatomic molecules is confirmed to be valid.

Funding sources

This work was financed by the French region Rhônes Alpes Auvergne (Optolyse, CPER2016).

Disclosures

The authors declare no conflicts of interest.

CRediT authorship contribution statement

Arsene Chemin: Methodology, Investigation, Formal analysis, Visualization, Software, Writing - Original Draft. **Amanda Ross**: Validation, Writing - Review & Editing. **Sylvain Hermelin**: Methodology, Writing -

Review & Editing. **Patrick Crozet**: Validation, Writing - Review & Editing. **Vincent Motto-Ros**: Conceptualization, Methodology, Validation, Writing - Review & Editing. **Gilles Ledoux**: Conceptualization, Methodology, Writing - Review & Editing. **Christophe Dujardin**: Funding acquisition, Writing - Review & Editing. **David Amans**: Conceptualization, Visualization, Data Curation, Software, Writing - Original Draft, Supervision.

Declaration of Competing Interest

The authors declare that they have no known competing financial interests or personal relationships that could have appeared to influence the work reported in this paper.

Data availability

Data will be made available on request.

Appendix A. Supplementary material

The supplementary materials describes the energy level calculations, including the parameters used, and the transition probability calculation. It also shows the plasma emission spectra at 5 μs and 30 μs with their fits.

References

[1] A. De Giacomo, J. Hermann, Laser-induced plasma emission: from atomic to molecular spectra, J. Phys. D 50 (2017) 183002. doi:10.1088/1361-6463/aa6585.

[2] S. S. Harilal, M. C. Phillips, D. H. Froula, K. K. Anoop, R. C. Issac, F. N. Beg, Optical diagnostics of laser-produced plasmas, Rev. Mod. Phys. 94 (2022) 035002. doi:10.1103/RevModPhys.94.035002.

[3] J. Hermann, E. Axente, F. Pelascini, V. Craciun, Analysis of multi-elemental thin films via calibration-free laser-induced breakdown spectroscopy, Analytical chemistry 91 (2019) 2544–2550. doi:10.1021/acs.analchem.8b05780.

[4] E. Tognoni, G. Cristoforetti, S. Legnaioli, V. Palleschi, Calibration-free laser-induced breakdown spectroscopy: state of the art, Spectrochimica Acta Part B: Atomic Spectroscopy 65 (2010) 1–14. doi:10.1016/j.sab.2009.11.006PANIST.

[5] T. E. Itina, J. Hermann, P. Delaporte, M. Sentis, Laser-generated plasma plume expansion: Combined continuous-microscopic modeling, Physical Review E 66 (2002) 066406. doi:10.1103/PhysRevE.66.066406.

[6] A. Chemin, K. Miyajima, P. Melinon, F. Mafuné, D. Amans, Microcanonical nucleation theory for anisotropic materials validated on alumina clusters, The Journal of Physical Chemistry A 124 (2020) 2328–2334. doi:10.1021/acs.jpca.0c01038.

[7] T. E. Itina, On nanoparticle formation by laser ablation in liquids, The Journal of Physical Chemistry C 115 (2011) 5044–5048. doi:10.1021/jp1090944.

[8] J. Lam, D. Amans, C. Dujardin, G. Ledoux, A.-R. Allouche, Atomistic mechanisms for the nucleation of aluminum oxide nanoparticles, J. Phys. Chem. A 119 (2015) 8944–8949. doi:10.1021/acs.jpca.5b05829.

[9] C. Alvarez, J. Pisonero, N. Bordel, Quantification of fluorite mass-content in powdered ores using a laser-induced breakdown spectroscopy method based on the detection of minor elements and caf molecular bands, Spectroc. Acta B 100 (2014) 123–128. doi:10.1016/j.sab.2014.07.024PANIST.

[10] O. Forni, M. Gaft, M. J. Toplis, S. M. Clegg, S. Maurice, R. C. Wiens, N. Mangold, O. Gasnault, V. Sautter, S. Le Mouelic, P.-Y. Meslin, M. Nachon, R. E. McInroy, A. M. Ollila, A. Cousin, J. C. Bridges, N. L. Lanza, M. D. Dyar, First detection of fluorine on mars: Implications for gale crater's geochemistry, Geophys. Res. Lett. 42 (2015) 1020–1028. doi:10.1002/2014GL062742.

[11] J. C. Polanyi, K. B. Woodall, Mechanism of rotational relaxation, J. Chem. Phys. 56 (1972) 1563. doi:10.1063/1.1677406.

[12] H. P. Broida, T. Carrington, Rotational, vibrational, and electronic energy transfer in fluorescence of nitric oxide, J. Chem. Phys. 38 (1963) 136. doi:10.1063/1.1733452.

[13] J. Jones, K. Richter, T. J. Price, A. J. Ross, P. Crozet, C. Faust, R. F. Malenda, S. Carlus, A. P. Hickman, J. Huennekens, Rotationally inelastic collisions of excited nak and nacs molecules with noble gas and alkali atom perturbers, J. Chem. Phys. 147 (2017) 144303. doi:10.1063/1.4997577.

[14] J. Lam, V. Motto-Ros, D. Misiak, C. Dujardin, G. Ledoux, D. Amans, Investigation of local thermodynamic equilibrium in laser-induced plasmas: Measurements of rotational and excitation temperatures at long time scales, Spectroc. Acta B 101 (2014) 86–92. doi:10.1016/j.sab.2014.07.013PANIST.

[15] P. Ran, H. Hou, S.-N. Luo, Molecule formation induced by non-uniform plume–air interactions in laser induced plasma, J. Anal. At. Spectrom. 32 (2017) 2254–2262. doi:10.1039/C7JA00287D.

[16] E. R. Wainwright, S. W. Dean, F. C. De Lucia, T. P. Weihs, J. L. Gottfried, Effect of sample morphology on the spectral and spatiotemporal characteristics of laser-induced plasmas from aluminum, Applied Physics A 126 (2020) 83. doi:10.1007/s00339-019-3201-9.

[17] S. S. Harilal, B. E. Brumfield, B. D. Cannon, M. C. Phillips, Shock wave mediated plume chemistry for molecular formation in laser ablation plasmas, Analytical chemistry 88 (2016) 2296–2302. doi:10.1021/acs.analchem.5b04136.

[18] C. G. Parigger, J. O. Hornkohl, Computation of AlO $B^2\Sigma^+ \rightarrow X^2\Sigma^+$ emission spectra, Spectroc. Acta Pt. A-Molec. Biomolec. Spectr. 81 (2011) 404–411. doi:10.1016/j.saa.2011.06.029PANIST.

[19] I. Kovacs, Rotational Structure in the Spectra of the Diatomic Molecules, Institute of Physics Publishing, London, 1969.

[20] I. G. Dors, C. Parigger, J. W. L. Lewis, Spectroscopic temperature determination of aluminum monoxide in laser ablation with 266-nm radiation, Opt. Lett. 23 (1998) 1778–1780. doi:10.1364/OL.23.001778.

[21] C. M. Western, Pgopher: A program for simulating rotational, vibrational and electronic spectra, J. Quant. Spectrosc. Radiat. Transf. 186 (2017) 221–242. doi:10.1016/j.jqsrt.2016.04.010PANIST.

[22] C. G. Parigger, A. C. Woods, D. M. Surmick, G. Gautam, M. J. Witte, J. Hornkohl, Computation of diatomic molecular spectra for selected transitions of aluminum monoxide, cyanide, diatomic carbon, and titanium monoxide, Spectroc. Acta Pt. B-Atom. Spectr. 107 (2015) 132–138. doi:10.1016/j.sab.2015.02.018PANIST.

[23] M. D. Saksena, M. N. Deo, K. Sunanda, S. H. Behere, C. T. Londhe, Fourier transform spectral study of $B^2\Sigma^+ - X^2\Sigma^+$ system of AlO, J. Mol. Spectrosc. 247 (2008) 47–56. doi:10.1016/j.jms.2007.10.002PANIST.

[24] P. J. Dagdigian, H. W. Cruse, R. N. Zare, Laser fluorescence study of alo formed in the reaction Al+O_2: Product state distribution, dissociation energy, and radiative lifetime, J. Chem. Phys. 62 (1975) 1824–1833. doi:10.1063/1.430710.

[25] S. Johnson, G. Capelle, H. Broida, Laser Excited Fluorescence and Radiative Lifetimes of AlO ($B^2\Sigma^+$-$X^2\Sigma^+$), J. Chem. Phys. 56 (1972) 663–665. doi:10.1063/1.1676921.

[26] L. Nagli, M. Gaft, Combining laser-induced breakdown spectroscopy with molecular laser-induced fluorescence, Appl. Spectrosc. 70 (2016) 585–592. doi:10.1177/0003702816631292.

[27] J. Lam, D. Amans, F. Chaput, M. Diouf, G. Ledoux, N. Mary, K. Masenelli-Varlot, V. Motto-Ros, C. Dujardin, γ-Al_2O_3 nanoparticles synthesised by pulsed laser ablation in liquids: a plasma analysis, Phys. Chem. Chem. Phys. 16 (2013) 963–973. doi:10.1039/C3CP53748J.

[28] G. Herzberg, Molecular Spectra and Molecular Structure, Volume I - Spectra of Diatomic Molecules, Krieger Publishing Company, Melbourne, 1950.

[29] P. F. Bernath, Spectra of Atoms and Molecules, 2nd Edition, Oxford University Press, New York, 2005.

[30] O. Launila, L.-E. Berg, Spectroscopy of AlO: Combined analysis of the $A^2\Pi_i \rightarrow X^2\Sigma^+$ and $B^2\Sigma^+ \rightarrow X^2\Sigma^+$ transitions, J. Mol. Spectrosc. 265 (2011) 10–14. doi:10.1016/j.jms.2010.10.005.

[31] G. R. Hebert, R. W. Nicholls, C. Linton, Absolute band strengths for the AlO blue-green ($B^2\Sigma^+ - X^2\Sigma^+$) band system, J. Quant. Spectrosc. Radiat. Transfer. 23 (1980) 229–235. doi:10.1016/0022-4073(80)90010-2.

[32] E. J. Kautz, M. C. Phillips, A. Zelenyuk, S. S. Harilal, Oxidation in laser-generated metal plumes, Physics of Plasmas 29 (2022) 053509. doi:10.1063/5.0090155.